Neptunium sorption and redox speciation at the illite surface under highly saline conditions

Nidhu Lal Banik, Rémi Marsac, Johannes Lützenkirchen, Christian Maquardt, Kathy Dardenne, Joerg Rothe, Kerstin Bender, Horst Geckeis

Neptunium sorption and redox speciation at the illite surface under highly saline conditions

Nidhu lal Banik[a,b], Rémi Marsac[a,c,*], Johannes Lützenkirchen[a], Christian Michael Marquardt[a], Kathy Dardenne[a], Joerg Rothe[a], Kerstin Bender[a] and Horst Geckeis[a]

Address:

[a] Institut für Nukleare Entsorgung, Karlsruhe Institute of Technology, P.O. Box 3640, D-76021 Karlsruhe, Germany.

Present addresses:

[b] JRC-KARLSRUHE, G.II.6 - Nuclear Safeguards and Forensics, European Commission, P.O.Box 2340, D-76125 Karlsruhe

[c] Géosciences Rennes UMR 6118, Université Rennes 1, CNRS, 35042 Rennes cedex, France.

*Corresponding author:

e-mail address: remi.marsac@univ-rennes1.fr

Tel: +332 23 23 53 56. Fax: +332 23 23 60 90

ABSTRACT. Neptunium (Np) uptake on illite is investigated in 1 and 3.2 molal (m) NaCl solutions under inert (Ar) atmosphere for $4 < pH_m < 10$ ($pH_m = - \log m_{H^+}$) and $5\times10^{-8} < [Np(V)]_{tot} < 3\times10^{-4}$ M. In agreement with a previous study in 0.1 m NaCl solutions [Marsac et al. (2015) Geochim. Cosmochim. Acta 152, 39-51], Np(V) is the prevailing oxidation state in the aqueous solution, but Np uptake by illite is affected by surface induced reduction. The extent of Np(V) reduction to Np(IV) follows the measured redox potential (or the $pe = - \log a_{e^-}$), which is influenced by the introduced Np(V) amount, because of the low redox capacity of the illite. The presence of Np(IV) on the solid phase is verified by X-ray Absorption Near Edge Spectroscopy (XANES). We can conclude that Np uptake by illite is not significantly affected by the variation of m_{NaCl} from 0.1 to 3.2 m and thus is in agreement with reports on tetravalent actinide and Np(V) sorption to clays at high ionic strength. The combination of (i) the two site protolysis non-electrostatic surface complexation and cation exchange model, (ii) the specific ion interaction theory to calculate activity coefficients for dissolved species and (iii) by accounting for redox equilibria and the stability of surface Np species, the overall Np uptake by illite can be simulated as a function of pH_m, pe and m_{NaCl} using a single set of parameters. The present experimental and modeling results are particularly important in the context of deep geological nuclear waste disposal since many sedimentary rocks or clay formations that are deemed suitable for this purpose exhibit highly saline porewaters.

Keywords: Neptunium, illite, redox, saline, high ionic strength, surface complexation, spectroscopy, geochemical modeling.

1. INTRODUCTION

The final disposal in deep geologic formations is considered the most appropriate strategy to isolate high level nuclear waste (HLW) from the biosphere (e.g. OECD/NEA, 2008). Sedimentary clay rock formations are potential host rocks for HLW in several European countries encompassing Opalinus Clay (OPA) in Switzerland (Nagra, 2002), Boom and Ypresian clays in Belgium (Ondraf, 2001), Callovo-Oxfordian (COx) clays in France (Andra, 2005) or Boda Claystone in Hungary (Lázár and Máthé, 2012). Indeed, clays exhibit low permeability, large surface areas and pronounced sorption capacity for many relevant radionuclides via ion exchange reactions as well as surface complexation to silanol and/or aluminol groups at the edges of clay particles. Illite and smectite are the most important components of the proposed claystone host rocks and may amount to about 50 wt.% of the material (Lauber et al., 2000; Gaucher et al., 2004; Bradbury and Baeyens, 2011; Pearson et al., 2011; Chen et al., 2014). Although actinide sorption to clays has been extensively studied (e.g. Bradbury and Baeyens, 2005; 2009a,b; and references therein), the underlying mechanisms were rarely investigated for ionic strengths above 0.1 M. While OPA and COx porewaters exhibit ionic strengths of 0.3-0.4 M, clay rock pore waters as e.g. in the Jurassic and lower Cretaceaous clay rock in Northern Germany, which are also discussed as potentially appropriate host rock formations, may contain salt contents as high as about 5 M (Brewitz, 1980). Sedimentary rocks currently investigated in Canada are even in contact with brine solutions up to 6.5 M (Fritz and Frape, 1982). Therefore, detailed sorption investigations and the development of geochemical models that can predict actinide sorption and speciation in concentrated brine solutions are required (Vilks, 2011).

Neptunium (Np) is a minor constituent of high level radioactive waste. Yet, its environmental chemistry is of considerable interest due to the long half-life of its main isotope ^{237}Np ($t_{1/2}$ = 2×10^{6} a) and the high solubility and mobility of its pentavalent state

71 (NpO_2^+) under oxidizing conditions. Np is redox sensitive and its most relevant oxidation
72 states in the geosphere are the penta- and tetravalent states (Kim, 1986). Both redox states
73 show drastically different geochemical behavior concerning, for instance, complexation by
74 organic and inorganic ligands, solubility, as well as sorption to minerals (e.g. Altmaier et al.,
75 2013). Under reducing conditions, Np(IV) prevails and is considered rather immobile because
76 of its strong sorption to minerals and its low solubility, as other tetravalent actinides (An; e.g.
77 Th(IV)) or other tetravalent elements (e.g. Sn(IV)) (Bradbury and Baeyens, 2009a,b). Under
78 oxidizing conditions, Np(V) prevails, which weakly sorbs to minerals and is regarded as
79 rather mobile (e.g. Geckeis et al., 2013). However, partial reduction of Np(V) to Np(IV) when
80 in contact with Opalinus Clay was suggested by comparing sorption data obtained under
81 aerobic and anaerobic conditions: stronger Np sorption (Fröhlich et al., 2011) was found
82 under anaerobic conditions and significant reduction to Np(IV) was observed using
83 synchrotron based spectroscopic techniques (Fröhlich et al., 2012). A more recent Np-illite
84 batch sorption study under oxygen-free argon atmosphere in 0.1 M NaCl showed that the
85 strongly adsorbing Np(IV) is thermodynamically favored at a mineral surface compared to
86 Np(V) (Marsac et al., 2015a). Although Np(V) prevailed in aqueous solution at pH ≈ 7, as
87 evidenced by liquid-liquid extraction method and by capillary electrophoresis hyphenated to
88 inductively coupled plasma mass spectrometry (Graser et al., 2015), Np(IV) was observed at
89 the illite surface by X-ray absorption near edge structure spectroscopy (XANES). When
90 accounting for the uptake of both Np(V) and Np(IV) on illite and the redox potential of the
91 illite suspension, Marsac et al. (2015a) were able to describe the overall Np uptake on illite
92 for various redox conditions. The modeling approach was subsequently extended to the
93 sorption behavior of plutonium, which exhibits an even more complex redox chemistry than
94 Np. Pu can be found in the redox states +III to +VI under environmental conditions. The
95 experimentally determined overall Pu uptake on kaolinite (Marsac et al., 2015b) and illite
96 (Banik et al., 2016) in 0.1 M $NaCl/ClO_4$ was successfully reproduced.

The above cited studies focused on aqueous solutions of low ionic strength. At high salt concentrations, activity coefficients of aqueous species change dramatically, whereas the effect of high ionic strengths on the surfaces properties of adsorbents and surface species is elusive. Previous work showed that non-electrostatic models are quite suitable to predict proton and metal ion sorption at high ionic strength to naturally occurring matrices that bear surface functional groups that are affected by pH and can be treated by the same formalism and with similar numerical models. This includes marine microalgae (Schjif and Herbling, 2010; Zoll and Schjif, 2012) or bacteria (Ams et al., 2013). Eu(III) sorption to illite and smectite was investigated experimentally in 0.1 < m_{NaCl} < 3.9 molal (m) (Schnurr et al., 2015). The results obtained in the latter study showed that the 2 site protolysis non-electrostatic surface complexation and cation exchange (2 SPNE SC/CE) model coupled to either the specific ion interaction theory (SIT; Ciavatta, 1980) or the Pitzer formalism (Pitzer, 1991) to account for activity coefficients in concentrated media was able to reproduce sorption data also at elevated ionic strength. By using the modeling approach of Schnurr et al. (2015), the Pu-illite study in 0.1 M NaCl of Banik et al. (2016) was extended to high ionic strength (0.1 < m_{NaCl} < 3.2 m; Marsac et al., 2017). In the latter studies, the Pu(IV)/Pu(III) is involved. The present study is a similar extension of the work of Marsac et al. (2015a) on Np uptake on illite in 0.1 M NaCl to highly saline conditions (up to m_{NaCl} = 3.2 m), but here a An(V)/An(IV) couple is involved. Together, the work of Marsac et al. (2017) and the present one should elucidate the actinide(III,IV,V) sorption and redox speciation at the illite surface under highly saline conditions. Classical batch experiments at various pH, total Np concentrations and m_{NaCl} = 1.0 and 3.2 m were performed, and the redox potential was monitored. XANES was applied to determine the Np redox state at the illite surface. The coupling of the 2 SPNE SC/CE model with SIT was used to describe Np sorption and redox speciation on illite under saline conditions.

123 ## 2. MATERIALS AND METHODS

124 All chemicals were of pro analytical quality or better and were obtained from Merck
125 (Darmstadt, Germany) or Riedel de Haen (Seelze, Germany). Experiments were conducted
126 with de-ionized "MilliQ" water (specific resistivity, 18.2 MΩ cm). The purified Na-illite was
127 provided within the EC project CP CatClay. The source material derives from lacustrine
128 continental sediments deposited at the Upper Eocene (~ -35 Ma) in the basin of Le Puy en
129 Velay (Massif Central, France). The purification procedures and the characterization of the
130 purified illite (<63 µm) were previously described in detail (Marsac et al., 2015). Concerning
131 redox processes, it is noted that the iron content is 0.88 mol Fe per kg of illite (Marsac et al.,
132 2015). The aqueous concentration of ^{237}Np in sorption experiments after phase separation was
133 determined by liquid scintillation counting (LSC) using the scintillation cocktail Ultima Gold
134 XR (Packard Instruments Co., USA) and the liquid scintillation counter (LSC) Tri-Carb
135 (Packard Instruments Co., USA). Results for ^{237}Np-α-activities were corrected for
136 interferences by the β-radiation from the daughter nuclide protactinium (^{233}Pa) by applying
137 the α/β discrimination method. The procedure is described in detail by Marsac et al. (2015a)
138 and will not be repeated here. ^{233}Pa is a short-lived isotope ($t_{1/2}$ = 27 days) unlike ^{237}Np ($t_{1/2}$ =
139 2.14 10^6 years). Since the ^{233}Pa mass concentration is much smaller than that of ^{237}Np, its
140 competitive effect on Np sorption to illite can be neglected.
141

142 ### 2.1. Neptunium stock solution

143 The initial ^{237}Np solution was evaporated to dryness and dissolved in 8 M HCl. The
144 solution was purified via anion exchange (BIO RAD® AG 1-X8). After a washing step with
145 several milliliters of 8 M HCl, Pu contaminations were removed with a fresh solution of 150
146 mg NH_4I in 5 mL 8 M HCl. Subsequently, Np was eluted from the ion exchanger with 4 M
147 HCl/0.05 M HF and evaporated to dryness in a PTFE beaker. The sample was fumed twice

with 1 M $HClO_4$ and the residue was dissolved in deionized water to obtain a solution containing only NpO_2^+, as required for all our experiments, and its purity was verified by UV-Vis/NIR spectroscopy (Sjoblom and Hindman 1951). The final Np concentration was determined by LSC.

2.2. Determination of pH and Eh

pH in the clay suspensions was measured by an Orion 525A pH meter and a Ross electrode calibrated with 4 standard buffers (pH 3, 5, 7 and 9; Merck). The uncertainty of pH measurements is ± 0.05. For converting the pH value measured in saline solutions (I > 0.1 m) (pH_{exp}) into a chemically meaningful quantity, a correction is applied in order to obtain the molal proton concentration, i.e. –log m_{H^+} (pH_m). An empirical correction coefficient (A) which has been accurately determined by Altmaier et al. (2003) for NaCl solutions for our set-up with known -log m_{H^+} was added to pH_{exp} values according to equations 1 and 2:

$$pH_m = pH_{exp} + A_{NaCl} \quad (1)$$

$$A_{NaCl} = 0.0013 \times m_{NaCl}{}^2 + 0.1715 \times m_{NaCl} - 0.0988 \quad (2)$$

where m_{NaCl} is the molality (mol kg^{-1}) of the background electrolyte.

The redox potentials in the clay suspensions were measured using an Orion 525A (E_h meter) and a Pt combined electrode with a Ag/AgCl reference (Metrohm). They were converted into Eh vs. standard hydrogen electrode (SHE) by correcting for the potential of the reference electrode. A commercial redox-buffer (220 mV, Schott instruments) was used for calibration. An equilibration time of 15 min was allowed for all Eh measurements, after having stirred the suspension. Uncertainties in Eh measurements are ± 50 mV (Altmaier et al., 2010; Kirsch et al., 2011). Eh was converted to the logarithm of the apparent electron activity, pe = -log a_{e^-} = 16.9×Eh(V) at 25°C. To our best knowledge, no ionic strength dependent correction needs to be performed for experimentally measured Eh values (as the one that has been described for pH measurements in brines above).

2.3. Batch sorption experiments

All sorption experiments were performed as batch type experiments with initial Np(V) concentrations in the range of 5×10^{-8}- 3×10^{-6} M. The batch experiments were carried out in 40 mL polypropylene centrifuge tubes at room temperature in an argon glove box (< 1 ppm O_2, absence of CO_2). The sample volume was 25 mL. At a solid-to-liquid ratio of 2 g L^{-1}, the suspensions were preconditioned at a given m_{NaCl} under continuous shaking for 4-5 days to achieve a given target pH_m value by adding 0.1 M HCl or 0.1 M NaOH. After mixing the NpO_2^+ solution with the preconditioned illite suspension, pH_m was readjusted by adding acid or base (HCl/NaOH). The samples were shaken end-over-end. According to Marsac et al. (2015a), Np(V) adsorption or reduction to Np(IV) does not significantly change with time after 7 days. Therefore, after 7 days, pH_m and Eh were measured in the suspension and an aliquot of each sample was centrifuged in a Beckman L7 Ultracentrifuge at 90000 rpm for 1 h. The supernatant was analyzed for dissolved Np by LSC. Results obtained in batch experiments will be expressed throughout as distribution coefficients (R_d in L kg^{-1}), calculated by the following equation:

$$R_d = \left([Np]_{tot}/[Np]_{aq} - 1\right) \times V/m \quad (3)$$

where $[Np]_{aq}$ and $[Np]_{tot}$ (mol L^{-1}) are the dissolved (final) equilibrium and total (initial) concentrations of Np in solution, respectively. The term V/m corresponds to the aqueous solution volume to illite mass ratio (L kg^{-1}). An uncertainty of ± 0.3 is commonly associated with log R_d determined for radionuclide sorption to clay minerals (Bradbury and Baeyens, 2009a), although for low $[Np]_{tot}$ and high uptake, the uncertainty on log R_d might be larger.

2.4. X-ray absorption near-edge spectroscopy (XANES)

One sample was prepared as described in the previous section for Np L_3-XANES measurements for $[NpO_2^+]_{tot}$ = 3×10^{-4} M, m/V = 20 g L^{-1}, $\boldsymbol{m_{NaCl}}$ = 3.2 and pH_m = 7.9 under

197 inert (Ar) atmosphere. The Eh measured after one week equilibration time was 0.43 ± 0.05 V
198 (pe = 7.3 ± 0.8). A similar experiment is described in Marsac et al. (2015a), however,
199 performed in 0.1 m NaCl and at Eh = 0.40 ± 0.05 V (pe = 6.8 ± 0.8). Conditions for XANES
200 measurements and the data treatment were identical to what has been described in detail in
201 Marsac et al. (2015a). Briefly, an aliquot was centrifuged at 3000 g in a polyethylene vial
202 (500 µL). The supernatant was discarded, but an aliquot was taken for LSC. The wet illite
203 paste was transferred into a vial, mounted inside an Ar-flushed cell, which acts as a second
204 containment and keeps the sample vials in an anaerobic atmosphere (Brendebach et al., 2009).
205 Measurements were performed at the 2.5 GeV synchrotron light source ANKA, KIT,
206 Germany, at the INE-Beamline for actinide research (Rothe et al., 2006; 2012). A pair of
207 Ge(422) crystals was used in the Lemonnier-type double crystal monochromator (DCM). The
208 monochromatic radiation is focused by a Rh-coated toroidal mirror to a spot of < 1 mm $\times$ 1
209 mm at the sample position. Higher harmonic radiation in the incident beam was suppressed by
210 detuning the parallel alignment of the DCM crystals to 70 % of photon flux peak intensity in
211 the middle of the spectral range at the beginning of each scan. The incident flux was measured
212 by an Ar-filled ionization chamber at ambient pressure and held constant by a digital
213 MOSTAB feedback system. The Np L_3-edge spectra ($E(Np^0\ 2p_{3/2})$ = 17.61 keV) were
214 calibrated against the first derivative XANES spectrum of a Zr foil (energy of the first
215 inflection point set to $E(Zr^0\ 1s)$ = 17.998 keV). All Np L_3-XANES spectra were recorded in
216 fluorescence detection mode by registering the Np L_α fluorescence yield at ~13.95 keV as a
217 function of the incident photon energy with a 5-pixel Ge solid state detector (Canberra LEGe).
218 Up to 5 scans were collected at room temperature and averaged for each sample. The
219 illuminated area of the sample was changed between each scan to minimize potential Np
220 redox reactions induced by the beam. XANES spectra were extracted following subtraction of
221 a linear pre-edge background function and normalization of the edge jump to unity using the
222 Demeter Athena software (Ravel and Newville, 2005). The same energy range was

considered for the pre-edge and for the normalization of all XANES spectra (pre-edge: 17.30-17.55 keV; post-edge: 17.77-18.20 keV). Preliminary tests ensured that the differences in the XANES were not due to the normalization procedure.

2.5. Thermodynamic modeling

pe-pH diagrams for Np were obtained using PhreePlot (Kinniburgh and Cooper, 2009), which contains an embedded version of the geochemical speciation program PHREEQC (Parkhurst and Appelo, 1999). PhreePlot also includes a parameter optimization procedure, which allows fitting a model to experimental data by minimizing the weighted sum of squares of the residuals. Thermodynamic constants for Np aqueous speciation were taken from the NEA thermodynamic database (Guillaumont et al., 2003). The specific ion interaction theory (SIT; Ciavatta, 1980) was used for the calculation of the activity coefficients of aqueous species. The 2 SPNE SC/CE model was used to simulate Np sorption to illite (Bradbury and Baeyens, 2009b). Cation exchange reactions of a metal ion with a charge +n (M^{n+}) on Na-illite can be written as follows (Gaines and Thomas, 1953):

$$M^{n+} + n\ \text{Na-Illite} \rightleftharpoons n\ Na^{+} + \text{M-Illite} \quad (4)$$

The cation exchange capacity (CEC) of the illite was set to 0.225 eq/kg. Surface complexation reactions can be written as follows:

$$\equiv SOH + M^{n+} + (x\text{-}1)\ H_2O = \equiv SOM(OH)_{(x-1)}^{(n-x)} + x\ H^{+}\ ;\ {}^{S}K_{(x-1)} \quad (5)$$

where M^{n+} is a metal ion with a charge of +n and $\equiv$SOH is a protonated surface site.

Only the least abundant, i.e. strong, sites of the 2 SPNE SC/CE model were considered in the adsorption calculations with a site density of 2×10^{-3} mol kg^{-1}, since the weak sites are irrelevant at trace levels of Np. Bradbury and Baeyens (2009b) determined a NpO_2^{+}-Na^{+} selectivity coefficient for illite as well as Np(V) surface complexation constants for illite within the 2 SPNE SC/CE model. Marsac et al. (2015a) determined surface complexation

constants for Np(IV). However, the fitted constants relied on the experimental Eh and, therefore, are subject to large uncertainties. Np and Pu are neighbors in the actinide series and the hydrolysis constants of Np(IV) and Pu(IV) are not significantly different (Guillaumont et al., 2003). On the basis of the linear free energy relationship determined for illite by Bradbury and Baeyens (2009b), the surface complexation constant for Np(IV) and Pu(IV) should not significantly differ. Recently, the surface complexation constants for Pu(IV) were refined for illite by Banik et al. (2016). The constants from the latter study were used here for Np(IV). No constants are available for Np(V) and Np(IV) surface complexation to the more abundant but weaker sites defined in the 2 SPNE SC/CE model. The complete aqueous thermodynamic database, SIT coefficients and the parameters for the 2SPNE SC/CE model are given in the supporting information.

3. RESULTS

3.1. Experimental batch results

Figure 1 presents experimental log R_d (R_d in L kg^{-1}) values versus pH_m for initial Np(V) concentrations of 10^{-6} M (Fig. 1a) and 5×10^{-8} M (Fig. 1b), and m_{NaCl} = 1.0 and 3.2 m. The results of Marsac et al. (2015a) in 0.1 m NaCl obtained after 1 week contact time are included for $[Np(V)]_{tot} = 10^{-6}$ M (Fig. 1a) and 3×10^{-8} M (Fig. 1b). No data are available for $[Np(V)]_{tot} = 5\times10^{-8}$ M in 0.1 m NaCl. For both values of $[Np(V)]_{tot}$, no clear effect of the ionic strength on Np sorption is observed. This is consistent with the results of experiments related to the sorption of Np(V) onto illite, shale and bentonite (MX80) in NaCl/$CaCl_2$ solutions up to I~4.7 M (Nagasaki et al., 2016). For $[Np(V)]_{tot} = 10^{-6}$ M, log R_d slightly increases with pH_m whereas, for $[Np(V)]_{tot} = 3$ or 5×10^{-8} M, the increase in log R_d with pH_m is more pronounced. As observed by Marsac et al. (2015a), Np sorption to illite is stronger for low $[Np(V)]_{tot}$. By comparison with the uptake of other cations on illite, it was demonstrated that this behavior

cannot be due to site saturation effects (see Figure 2 and corresponding text in Marsac et al., 2015a). In 0.1 m NaCl, the observations for Np were explained by the relatively low pe measured in the suspension and the formation of Np(IV) at the illite surface, with Np(V) prevailing in the aqueous solution. By addition of 10^{-6} M Np(V) the overall concentration of oxidants in the suspension increases and apparently overcompensates the relatively low redox capacity of the illite suspension. As a consequence, pe increases and a smaller fraction of Np(V) is reduced to Np(IV), which explains the observed reduced Np uptake at high $[Np(V)]_{tot}$. Our results must be interpreted by taking into account the actual redox conditions in the system. Figure 2 shows the complete datasets for various $[Np(V)]_{tot}$ (0.05, 0.09, 0.3, 0.5, 0.9 and 3 µM) in 1.0 m (Fig. 2a,b) and 3.2 m NaCl (Fig. 2c,d). On the left side (Fig. 2a,c), uptake data are shown as log R_d versus pH_m whereas, on the right side (Fig. 2b,d), the corresponding pe versus pH_m data are given. As expected, the samples with the highest $[Np(V)]_{tot}$ show the highest pe and the lowest log R_d, whereas the highest log R_d values are measured at the lowest pe and the lowest $[Np(V)]_{tot}$. Although a small amount of Fe(II) contained in the illite was supposed to be responsible for the reduction of Np(V) to Np(IV) (Marsac et al. (2015a)), this could not be monitored experimentally. As calculated in the latter study, the amount of Fe(II) required for the reduction of Np(V) in the most concentrated sample (i.e. XANES sample: $[Np(V)]_{tot} = 3\times10^{-4}$ M; 20 g/L illite) corresponds to about 0.08 % of the total amount of Fe contained in the illite. Such small fractions are very likely below the detection limit of available experimental techniques.

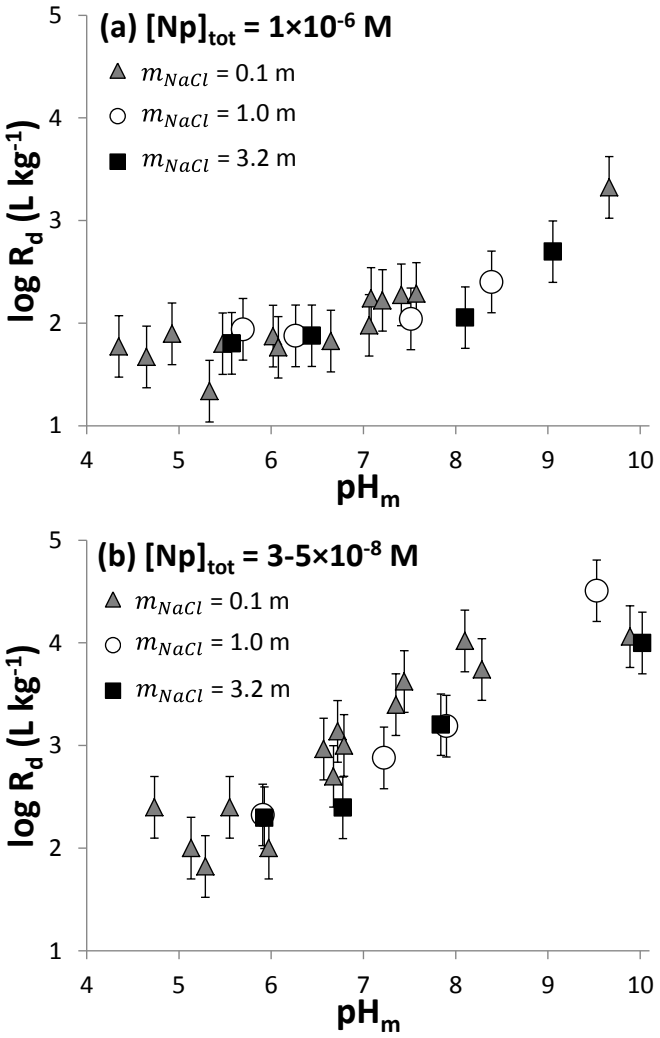

Figure 1. Np sorption to illite (log R_d in L kg^{-1}) after 1 week contact time in 1.0 and 3.2 m NaCl versus pH_m for $[Np(V)]_{tot} = 10^{-6}$ M (a) and 5×10^{-8} M (b). The results obtained in 0.1 m NaCl are taken from Marsac et al. (2015a) after 1 week contact time, $[Np(V)]_{tot} = 10^{-6}$ M (a) and 3×10^{-8} M (b).

3.2. Simulation of Np(V) and Np(IV) uptake

Calculations are made using the 2 SPNE SC/CE model in combination with SIT and the surface complexation constants for Np(V) and Pu(IV) determined by Bradbury and Baeyens (2009b) and Banik et al. (2016), respectively, for $[NaCl/ClO_4] \leq 0.1$ m. Np(IV) sorption is considered to be identical to that of Pu(IV). The model is used to calculate the uptake of Np(V) and Np(IV) without considering redox transitions. Results are shown in figure 2a (for 1 m NaCl) and 2c (for 3.2 m NaCl). As for Pu(IV) (Marsac et al., 2017), no significant ionic strength effect on Np(IV) sorption onto illite is observed for $0.1 < m_{NaCl} <$

306 3.2 m. This is also consistent with the outcome of a previous study on Th(IV) sorption to
307 montmorillonite between 0.1 and 1 m $NaClO_4$ (Bradbury and Baeyens, 2005). Also the Np(V)
308 surface complexation to illite is found to be weakly affected by ionic strength for 0.1 < m_{NaCl}
309 < 3.2 m (see also Nagasaki et al., 2016). As all metal ions, Np(V) is known to sorb to illite via
310 cation exchange at low pH (pH < 6; for Np(V)) and at pH > 6 via inner sphere complexation.
311 However, due to the small charge of the NpO_2^+ ion, and the multiple excess of Na^+
312 concentration, cation exchange becomes negligible and hence ionic strengths effects are not
313 pronounced. In figures 2a (for 1 m NaCl) and 2c (for 3.2 m NaCl), our experimentally
314 determined log R_d values lie between those calculated for Np(V) and Np(IV) sorption data.
315

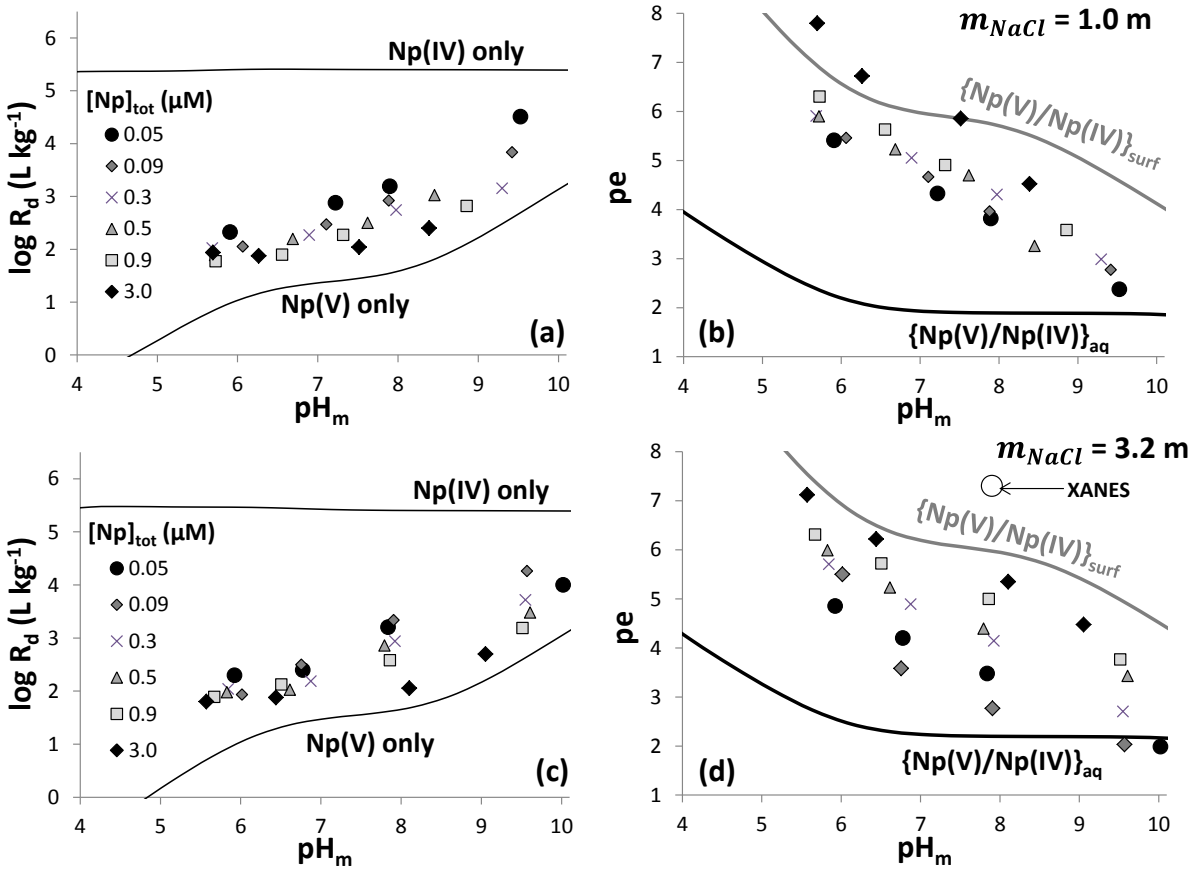

316

317 **Figure 2.** On the left: experimental log R_d data measured after 1 week versus the pH_m for the various $[Np]_{tot}$
318 investigated (0.05, 0.09, 0.3, 0.5, 0.9 and 3 µM; shown as different symbols), for m_{NaCl} = 1.0 m (a) and 3.2 m
319 (c). Calculated pH-edges for sorption of Np(V) and Np(IV) (no redox transition considered), respectively, are
320 shown as lines. On the right: corresponding pH_m-pe values measured in m_{NaCl} = 1.0 m (b) and 3.2 m (d) for the
321 different $[Np]_{tot}$ are shown with the same symbols as on the left. The calculated Np(V)/Np(IV) redox borderlines
322 in solution ($\{Np(V)/Np(IV)\}_{aq}$; black line) and at the illite surface ($\{Np(V)/Np(IV)\}_{surf}$; grey line) are also shown.
323 Error bars are not shown for clarity but uncertainties for log R_d (a,c) lie in the range of ± 0.3 and for pe (b,d) in
324 the range of ± 0.8. The pH-pe value for the sample analyzed by XANES (m/V = 20 g L^{-1}; 3.2 m NaCl; $[Np]_{tot}$ =
325 3×10^{-4} M) is also shown (d).

326

327 ***3.3. pH-pe diagrams in solution and at the illite surface***

328 Redox borderlines between the predominance fields of Np(V) and Np(IV) in solution
329 (noted as $\{Np(V)/Np(IV)\}_{aq}$) are shown in figures 2b (for 1.0 m NaCl) and 2d (for 3.2 m
330 NaCl) as black lines. The borderline between the predominance fields of Np(V) and Np(IV)
331 species adsorbed at the surface of illite (noted as$\{Np(V)/Np(IV)\}_{surf}$) is described by:

332 $$\{Np(V)/Np(IV)\}_{surf} = \{Np(V)/Np(IV)\}_{aq} + (\log R_d(Np(IV)) - \log R_d(Np(V))) \quad (6)$$

and is plotted as well in figures 2b and 2d (grey lines). In eq. 6, $\{Np(V)/Np(IV)\}_{aq}$ and $\{Np(V)/Np(IV)\}_{surf}$ correspond to pe values, where $[Np(V)]_{aq}/[Np(IV)]_{aq}$ and $[Np(V)]_{surf}/[Np(IV)]_{surf}$ equal 1. They can vary with physico-chemical conditions (pH_m, m_{NaCl}, T, etc) in a similar way as log R_d(Np(IV)) and log R_d(Np(V)).

As shown in previous studies (Marsac et al., 2015a,b; Banik et al., 2016; Marsac et al., 2017), the stability fields of surface sorbed Np(IV) and Pu(IV) species are extended relative to those for dissolved species because of their stronger sorption relative to that of other redox states (i.e. Pu(III,V,VI); Np(V)) under the conditions investigated in those studies. For pH < 6, at elevated ionic strength (i.e. 1.0 and 3.2 m), we find a shift of $\{Np(V)/Np(IV)\}_{surf}$ to significantly higher values because Np(V) sorption to illite is decreased. Np(V) and Np(IV) inner-sphere surface complexation to illite is only weakly affected by ionic strength so that $\{Np(V)/Np(IV)\}_{surf}$ hardly varies between 0.1 and 3.2 m NaCl for pH > 6.

By comparing the experimental pH_m-pe values and the calculated values for $\{Np(V)/Np(IV)\}_{aq}$ and $\{Np(V)/Np(IV)\}_{surf}$, we expect Np(V) to prevail in solution while Np(IV) predominantly exists as surface species. This qualitatively explains why the measured Np sorption data lie between those calculated for pentavalent and tetravalent Np species.

3.4. Spectroscopic results

Np redox speciation at the illite surface was further investigated by XANES for pH_m = 7.9 (pe = 7.3 ± 0.8), m/V = 20 g L^{-1}, 3.2 m NaCl and 3×10^{-4} M Np (introduced as NpO_2^+). In figure 3, the XANES spectrum recorded for the Np-illite sample prepared in 3.2 m NaCl is compared to the spectrum recorded in m_{NaCl} = 0.1 m by Marsac et al. (2015a) under similar conditions (pH_m = 7.4; pe = 6.8 ± 0.8). As explained before, phase separation was performed to remove the solution from the sample. Therefore, the following analysis of spectra pertains only to Np species associated to the solid phase. The Np-illite XANES spectra are compared to those reported for Np^{4+} and NpO_2^+ aquo ions in 0.1 M $HClO_4$ (Gaona et al., 2012),

measured at the same beamline. The presence of a shoulder at 17625 eV indicates multiple scattering of the outgoing Np $2p_{3/2}$ electrons along the axis of the NpO_2^+ dioxo cation. This indicates the prevalence of the +V redox state in both Np-illite samples. The "white line" (WL) position as well as the inflection point of Np redox states +IV and +V are similar and cannot be used as a conclusive probe for Np redox speciation. However, Np(V) and Np(IV) XANES show significant differences in the intensity of the WL. The WL intensity increases from the NpO_2^+ aquo ion to the Np-illite sample in 0.1 m NaCl. The sample prepared in 3.2 m NaCl shows intermediate intensity. As discussed in more detail in Marsac et al. (2015a) and Denecke et al. (2005), the WL of Np(V) sorbed to a mineral surface will be less intense than that of the Np(V) aquo-ion. Therefore, the present results indicate the presence of Np(IV). By fitting the 0.1 m NaCl Np-illite XANES spectrum with a linear combination of Np(V) and Np(IV) reference samples (i.e. aquo-ions), Marsac et al. (2015a) found that 14±1% (error provided by the Demeter Athena software; Ravel and Newville, 2005) of the adsorbed Np was Np(IV) (i.e. Np(V)-to-Np(IV) concentration ratio at the illite surface $[Np(V)]_{surf}/[Np(IV)]_{surf}$ = 6.1). Repeating the same exercise for the 3.2 m NaCl sample yields the presence of at least 8±1% of the Np existing as tetravalent species at the illite surface (i.e. $[Np(V)]_{surf}/[Np(IV)]_{surf}$ = 11.5). Although this value is small, it must be considered as a minimum value since the aquo-ions exhibit the most intense WLs. The same exercise with either a Np(V) or a Np(IV) reference, where Np is in a more condensed state (i.e. with a less intense WL), would lead to a larger fraction of Np(IV) (Marsac et al., 2015a). XANES analysis, therefore, yields a similar result compared to what has been obtained for the experiment at low ionic strength and provides a clear indication for partial reduction of Np(V), also at elevated ionic strength. Using experimental pe and spectroscopically determined $[Np(V)]_{surf}/[Np(IV)]_{surf}$ values, we find that $\{Np(V)/Np(IV)\}_{surf}$ = 6.0 (for m_{NaCl} = 0.1) and 6.2 (for m_{NaCl} = 3.2). These values compare very well with $\{Np(V)/Np(IV)\}_{surf}$ = 5.9 (for both 0.1 and 3.2 m NaCl), as determined by modeling (see e.g. the grey lines in Fig. 2b,d). This further confirms that the

Np(V)-Np(IV) redox transition at the illite surface is not substantially affected by ionic strength.

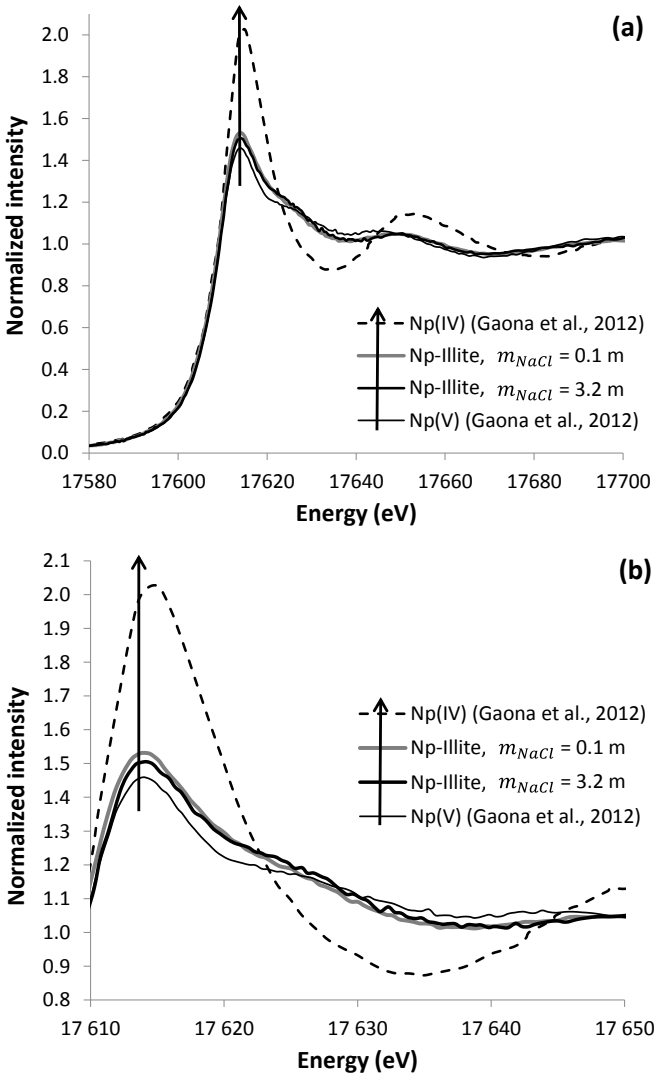

Figure 3. (a) Np L_3-XANES measured for Np-illite samples ($[Np]_{tot} = 3\times10^{-4}$ M, m/V = 20 g L^{-1}) prepared in 0.1 m NaCl (pH_m = 7.4; pe = 6.8; Marsac et al., 2015a) and 3.2 m NaCl (pH_m = 7.9; pe = 7.3; present study). Reference XANES of aqueous Np(IV) and Np(V) in 1 M $HClO_4$ from Gaona et al. (2012) are shown for comparison. Arrows highlight the partial Np(V) reduction to Np(IV) in the present study. The area between 17610 and 17650 eV is enlarged in (b). Results of the linear combination fit are shown in the supporting information (Figure S1).

4. DISCUSSION

4.1. Effects of pH_m, pe and m_{NaCl} on Np sorption to illite

Because Np uptake on illite is sensitive to pH_m and pe, it appears difficult to study in detail the effect of a third parameter, namely m_{NaCl}. Figure 4 shows data for experimentally determined log R_d plotted versus pe for m_{NaCl} = 0.1, 1.0 and 3.2. It is obvious that there is a strong correlation between R_d and pe showing that increasing the pe from 2 to 6 reduces R_d by ~ 3 orders of magnitude. In so far "pe edges" (log R_d plotted vs. pe) are more informative than the "pH edges" in Figures 2a and 2c (log R_d vs. pH). It appears that pe is the more relevant parameter determining Np retention under given conditions. A few experimental data do not fit into the trend and have been excluded from figure 4: (i) sorption data obtained at pH_m < 6 show a significant pH dependence because the Np(V)/Np(IV) borderlines in this range clearly evolve with pH (see Fig. 2b,d); (ii) at quite high pe values, where Np(V) prevails in solution and at the illite surface, the influence of pH on Np sorption is of course dominant (see the pH-edges of Np(V) in Fig. 2a,c). The exclusion of data points amount to ~20% of the complete data set, and make sure that, for the selected data, pH has no significant effect.

Figure 4 seems to suggest that Np sorption to illite is stronger in 0.1 than in 1.0 and 3.2 m NaCl at least for pe < 4.5, an issue that does not occur on Figure 1. Recent experimental investigations did not show significant influence of ionic strength neither on tetravalent actinide ion (I = 0.1 – 3.2 m; Bradbury and Baeyens, 2005; Marsac et al., 2017; results of both studies on Th(IV) and Pu(IV) sorption are shown in the supporting information) nor on Np(V) sorption to illite via inner-sphere surface complexation (I = 0.1 to 4.6 M; Nagasaki et al., 2016). Moreover, our XANES results suggest no ionic strength effect on Np(V)-Np(IV) redox transition at the illite surface. In fact, the interpretation of the Np-illite results is strongly affected by the experimental pe. Unlike Np, Th(IV) is not a redox sensitive metal ion and its sorption on illite is independent of the ionic strength within the experimental uncertainties.

The same independency of the ionic strength is observed for Pu(IV) illite uptake. From these results it would appear difficult to assume, that the ionic strength has no significant influence on the Np(IV) uptake, although trends in average values could suggest such effects. Therefore, it is more probable that the variations of Np-illite uptake data are due to the uncertainties of experimental pe measurements.

To highlight the consistency between Np-illite and Pu-illite sorption data in 0.1, 1.0 and 3.2 m NaCl (Banik et al., 2016; Marsac et al., 2017; present study), simulations are made with the 2 SPNE SC/CE model for pH_m = 7 and the results are plotted in Figure 4. This pH_m value is arbitrarily chosen because insignificant pH_m effect is expected for the selected dataset, as explained above. The surface complexation constant for Np(IV) given by Marsac et al. (2015a) (Table S3) describes sorption data determined for low ionic strength accurately, but overestimates sorption when comparing with experimental data determined in this study. In this case, log R_d(Np(IV)) = 6.1 (i.e. log R_d values extrapolated to pe values where all Np(V) in the system is reduced to Np(IV) in solution and at the illite surface). Adjusting model parameters to fit our data in 1.0 and 3.2 m NaCl using PhreePlot leads to log R_d(Np(IV)) = 4.7 (corresponding surface complexation constants are given in Table S3). In average, the model would give log R_d(Np(IV)) = 5.4 ± 0.7 (which is also determined by Phreeplot when using the complete dataset in 0.1, 1.0 and 3.2 m NaCl; Table S3). This average value is in excellent agreement with log R_d(Pu(IV)) = 5.3 ± 0.3 L kg^{-1} determined by Marsac et al. (2017) for 0.1 < m_{NaCl} < 3.2 m. Figure 4 shows that calculated log R_d evolves linearly with pe for intermediate pe values (for $\{Np(V)/Np(IV)\}_{aq}$ < pe < $\{Np(V)/Np(IV)\}_{surf}$, all the selected data are within this range in Figure 4). Therefore, an error of ±0.8 on pe leads to an error of ±0.8 on the calculated log R_d value, which compares well with the error on determined log R_d(Np(IV)) using Np-illite data at 0.1, 1 and 3.2 m NaCl (±0.7). These results suggest that it is reasonable to impose surface complexation constants for Np(IV) equal to those of Pu(IV)

and to attribute the trend of average Np-illite uptake with ionic strength effects to uncertainties in pe.

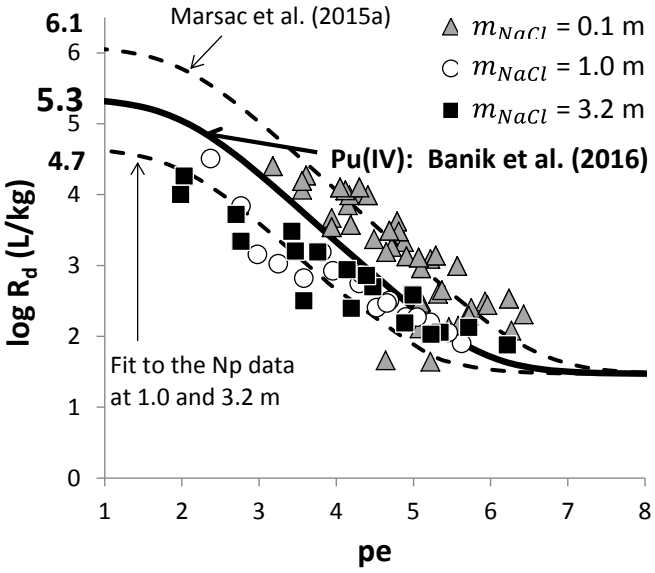

Figure 4. Np-illite sorption datasets from Marsac et al. (2015a; m_{NaCl} = 0.1 m) and the present study (m_{NaCl} = 1.0 and 3.2 m) are plotted as log R_d versus pe. Lines are calculations made with the 2 SPNE SC/CE model for pH_m = 7 using the surface complexation constants determined by Marsac et al. for Np(IV) (2015a; top dotted line), Banik et al. for Pu(IV) (2016; bold line) or fitting these constants to the 1.0 and 3.2 m NaCl data (bottom dotted curve). The corresponding log R_d(Np(IV)) is given on the y-axis.

4.2. Modeling An(III,IV,V) sorption to illite as a function of pH_m, pe and m_{NaCl}

Values of log R_d are calculated for all the presently investigated conditions (including the conditions of Marsac et al., 2015a) using the experimental pH_m and pe values. The model results are plotted versus the experimental log R_d in Figure 5. The results of Banik et al. (2016; 0.1 m NaCl) and Marsac et al. (2017; 1.0 and 3.2 m NaCl), involving the Pu(IV)/Pu(III) couple, are also included. The 1:1 line shows the good agreement between model and experiment. Deviations of ±1.1 log R_d unit are shown as dotted lines. This error for the calculated log R_d accounts for both the error on pe (±0.8) and on experimental log R_d (±0.3). For a wide range of pH_m, $[Np/Pu]_{tot}$, m_{NaCl} and pe investigated in these different studies (i.e. 179 experimental log R_d values) the discrepancies between model and the experimental

results rarely exceed 1.1 log R_d unit. The mean value of the deviation between experimental and calculated log R_d values is 0.42. It is important to note that sorption data are highly sensitive to the redox conditions and pe measurements are associated with considerable uncertainties. We nevertheless conclude that the combination of (i) the 2 SPNE SC/CE model, (ii) SIT and (iii) the approach developed by Marsac et al. (2015a,b), which accounts for redox equilibria and the stability of surface species, allows to reasonably model actinide(III,IV,V) uptake by illite as a function of pH_m, pe and m_{NaCl} up to highly saline conditions.

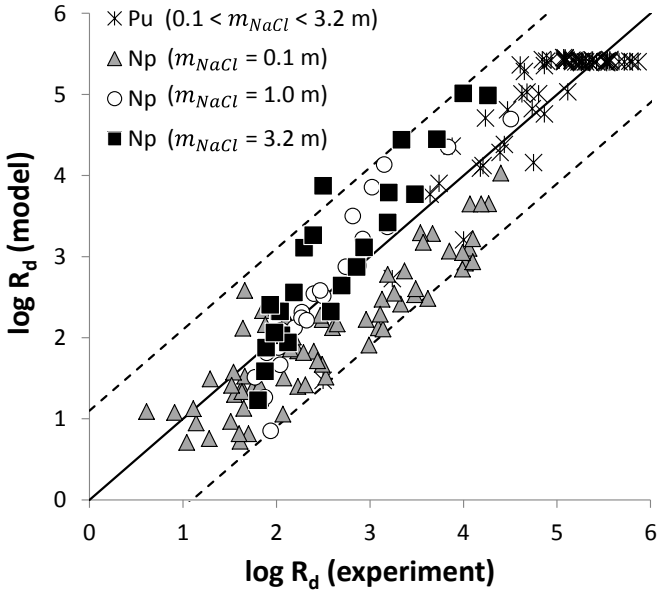

Figure 5. Modelled versus experimental log R_d values for Np (data from this study and Marsac et al., 2015a) and Pu in 0.1 < m_{NaCl} < 3.2 m (data from Banik et al., 2016; Marsac et al., 2017). The 1:1 (solid) line is associated with an uncertainty of ± 1.1 log R_d units (dashed lines).

4. CONCLUSIONS

In agreement with previous studies performed at low ionic strength (Marsac et al., 2015a), Np sorption increases with decreasing redox potential also at high m_{NaCl} (up to 3.2 m). Using a combined batch sorption, spectroscopic and geochemical modeling approach, the strong interaction between Np and illite is attributed to the partial reduction of Np(V) to

Np(IV) at the illite surface driven by the higher thermodynamic stability of Np(IV) surface complexes as compared to Np(V) surface species. By the combination of the 2 SPNE SC/CE model with SIT, it is possible to reproduce experimentally obtained overall Np uptake data for illite as a function of pH_m, pe and m_{NaCl} using a single set of parameters. The ionic strength has a relatively small impact on sorption of both Np(V) and Np(IV). Main parameters driving the sorption behavior of redox sensitive actinides are pH_m and pe.

Notably the role of the redox potential on the uptake of redox sensitive actinides on minerals is to be considered when applying laboratory derived conditional R_d values for performance safety assessment purposes. The applicability of such data is only justified, if redox conditions in laboratory experiments and those expected in the real system are identical. This is not always the case as extraction of natural materials from deep environments, transport to the laboratory and experimental handling are technically challenging and redox conditions may change due to e.g. access of oxygen. However, if the pH and redox potentials of *in situ* and laboratory conditions are known, mechanistic models as proposed here, are capable of assessing the overall uptake of redox sensitive actinides by natural adsorbents with reasonable accuracy. In agreement with recent studies, the use of non-electrostatic models appears suitable for the prediction of metal ion sorption to various types of surfaces even at elevated ionic strength, e.g. marine microalgae (Zoll and Schjif, 2012), bacteria (Ams et al., 2013), illite (Schnurr et al., 2015; Marsac et al., 2017) or smectite (Schnurr et al., 2015). Accordingly, the 2 SPNE SC/CE model is a reliable predictive tool for performance safety assessment for clays even under elevated saline conditions.

ACKNOWLEDGEMENTS

This work was financed by the Federal Ministry of Economic Affairs and Energy (Germany) under contracts No. 02E10206 and 02E10961. The research leading to these

509 results has received funding from the European Union's European Atomic Energy
510 Community's (Euratom) Seventh Framework Program FP7/2007-2011 under grant agreement
511 n° 249624 (CATCLAY project).

512

513 **Supporting Information Available**

514 Additional material is provided in the supporting information section.

515

REFERENCES

Altmaier M., Gaona X. and Fanghänel T. (2013) Recent advances in aqueous actinide chemistry and thermodynamics. *Chem. Rev.* **113**, 901-943.

Altmaier M., Gaona X., Fellhauer D. and Buckau G. (2010) Intercomparison of redox determination methods on designed and near-neutral aqueous systems. KIT-SR 7572, Karlsruhe Institute of Technology, Karlsruhe.

Altmaier M., Metz V., Neck V., Müller R. and Fanghänel Th. (2003) Solid-liquid equilibria of $Mg(OH)_{2(cr)}$ and $Mg_2(OH)_3Cl{\bullet}4H_2O_{(cr)}$ in the system Mg-Na-H-OH-Cl-H_2O at 25°C. *Geochim. Cosmochim. Acta* **67**, 3595–3601.

Ams D. A., Swanson J. S., Szymanowski J. E. S., Fein J. B., Richmann M. and Reed D. T. (2013) The effect of high ionic strength on neptunium (V) adsorption to a halophilic bacterium. *Geochim. Cosmochim. Acta* **110**, 45–57.

Andra, Dossier 2005 Synthèse Évaluation de la faisabilité du stockage géologique en formation argileuse. 2005, Agence nationale pour la gestion des déchets radioactifs (Andra): Châtenay-Malabry, France. p. 241.

Banik N. L., Marsac R., Lützenkirchen J., Diascorn A., Bender K. Marquardt C. M. and Geckeis H. (2016) Sorption and redox speciation of plutonium on illite. *Environ. Sci. Technol.* **50**, 2092–2098.

Bradbury M. H. and Baeyens B. (2005) Modelling the sorption of Mn(II), Co(II), Ni(II), Zn(II), Cd(II), Eu(III), Am(III), Sn(IV), Th(IV), Np(V) and U(VI) on montmorillonite: Linear free energy relationships and estimates of surface binding constants for some selected heavy metals and actinides. *Geochim. Cosmochim. Acta* **69**, 875–892.

Bradbury M. H. and Baeyens B. (2009a) Sorption modelling on illite Part I: Titration measurements and the sorption of Ni, Co, Eu and Sn. *Geochim. Cosmochim. Acta.* **73**, 990–1003.

Bradbury M. H. and Baeyens B. (2009b) Sorption modeling on illite Part II: actinide sorption and linear free energy relationships. *Geochim. Cosmochim. Acta.* **73**, 1004–1013.

Bradbury M. H. and Baeyens B. (2011) Predictive sorption modelling of Ni(II), Co(II), Eu(IIII), Th(IV) and U(VI) on MX-80 bentonite and Opalinus Clay: A "bottom-up" approach, *Appl. Clay Sci.* **52**, 27–33.

Brendebach B., Banik N. L., Marquardt C. M., Rothe J., Denecke M. and Geckeis H. (2009) X- ray absorption spectroscopic study of trivalent and tetravalent actinides in solution at varying pH value. *Radiochim. Acta* **97**, 701–708.

Brewitz W. (1980) Zusammenfassender Zwischenbericht, GSF T 114.

Chen Z., Montavona G., Guo Z., Wang X., Razafindratsima S., Robinet J. C., Landesmana C. (2014) Approaches to surface complexation modeling of Ni(II) on Callovo-Oxfordian clayrock. *Appl. Clay Sci.* **101**, 369–380.

Ciavatta L. (1980). The specific interaction theory in the evaluating ionic equilibria. *Ann. Chim.* **70**, 551–562.

555 Denecke M. A., Dardenne K. and Marquardt C. M. (2005) Np(IV)/Np(V) valence
556 determinations from Np L3 edge XANES/EXAFS. *Talanta* **65**, 1008–1014.

557 Fritz P. and Frape S. K. (1982). Saline groundwaters in the Canadian shield – a first overview.
558 *Chem. Geol.* **36**, 179–190.

559 Fröhlich D. R., Amayri S., Drebert J. and Reich T. (2011) Sorption of neptunium(V) on
560 Opalinus Clay under aerobic/anaerobic conditions. *Radiochim. Acta* **99**, 71–77.

561 Fröhlich D. R., Amayri S., Drebert J., Grolimund D., Huth J., Kaplan U., Krause J. and Reich
562 T. (2012) Speciation of Np(V) uptake by Opalinus Clay using synchrotron microbeam
563 techniques. *Anal. Bioanal. Chem.* **404**, 2151–2162.

564 Gaines G. I. and Thomas H. C. (1953) Adsorption studies on clay minerals. II. A formulation
565 of the thermodynamics of exchange adsorption. *J. Phys. Chem.* **21**, 714-718.

566 Gaona X., Tits J., Dardenne K., Liu X., Rothe J., Denecke M. A., Wieland E. and Altmaier M.
567 (2012) Spectroscopic investigations of Np(V/VI) redox speciation in hyperalkaline
568 TMA-(OH, Cl) solutions. *Radiochim. Acta* **100**, 759–770.

569 Gaucher E., Robelin C., Matray J. M., Négrel G., Gros Y., Heitz J. F., Vinsot A., Rebours H.,
570 Cassagnabère A. and Bouchet A. (2004) ANDRA underground research laboratory:
571 interpretation of the mineralogical and geochemical data acquired in the Callovian–
572 Oxfordian formation by investigative drilling. *Phys. Chem. Earth* **29**, 55–77.

573 Geckeis H., Lützenkirchen J., Polly R., Rabung T. and Schmidt M. (2013) Mineral–water
574 interface reactions of actinides. *Chem. Rev.* **13** (2), 1016–1062.

575 Graser C.-H., Banik N. L., Bender K. A., Marquardt C. M., Marsac R., Monytoya, V. and
576 Geckeis H. (2015) Sensitive Redox speciation of elements relevant to nuclear waste
577 disposal by Capillary Electrophoresis hyphenated to inductively coupled plasma sector
578 field mass spectrometry. *Anal. Chem.* **87**, 9786–94.

579 Guillaumont R., Fanghänel Th., Fuger J., Grenthe I., Neck V., Palmer D. A. and Rand M. H.
580 (2003) Update on the chemical thermodynamics of Uranium, Neptunium, Plutonium,
581 Americium and Technetium, Mompean, F.J., Domenech-Orti, C., Ben-Said, K.,
582 OECD/NEA Data Bank, Eds., vol. 5 of Chemical Thermodynamics, Elsevier,
583 Amsterdam.

584 Kim J. I. (1986) Chemical behaviour of transuranic elements in natural aquatic systems. In:
585 Handbook on the Physics and Chemistry of the Actinides. (Freeman, A. J., ed.) Elsevier
586 Science Publishers, B. V., Amsterdam p. 413.

587 Kinniburgh D. G. and Cooper D. M. (2009) PhreePlot: Creating graphical output with
588 PHREEQC. <http://www.phreeplot.org>.

589 Kirsch R., Fellhauer D., Altmaier M., Neck V., Rossberg A., Fanghänel Th., Charlet L. and
590 Scheinost A. C. (2011) Oxidation state and local structure of plutonium reacted with
591 magnetite, mackinawite, and chukanovite. *Environ. Sci. Technol.* **45**, 7267–7274

592 Lauber M., Baeyens B. and Bradbury M. H. (2000) Physico-chemical characterisation and
593 sorption measurements of Cs, Sr, Ni, Eu, Th, Sn and Se on Opalinus Clay from Mont
594 Terri. PSI Technical Report 00-10, Paul Scherrer Institut, Villigen/Switzerland

Lázár K. and Máthé Z. (2012) Claystone as a potential hostr for nuclear waste storage, in "Clay minerals in nature - Their characterization, modification and application.", Marta Valaskova (Ed.), InTech, ISBN 978-953-51-0738-5.

Marsac R., Banik N. L., Diascorn A., Kupcik T., Lützenkirchen J., Marquardt C. M., Schäfer T., Schild D., Rothe J., Dardenne K. and Geckeis H. (2015a) Neptunium redox speciation at the illite surface. *Geochim. Cosmochim. Acta* **152**, 39–51.

Marsac R., Banik N. L., Lützenkirchen J., Buda R. A., Kratz J. V. and Marquardt C. M. (2015b) Modeling plutonium sorption to kaolinite: accounting for redox equilibria and the stability of surface species. *Chem. Geol.* **400**, 1–10.

Marsac R., Banik N. L., Lützenkirchen J., Diascorn A., Bender K., Marquardt C. M. and Geckeis H. (2017) Sorption and redox speciation of plutonium on illite under highly saline conditions. *J. Coll. Int. Sci.* **485**, 59–64.

Nagasaki S., Saito T. and Yang T. T. (2016) Sorption behavior of Np(V) on illite, shale and MX-80 in high ionic strength solutions. *J. Radioanal. Nucl. Chem.*, **308**, 143–153.

Nagra (2002) Project opalinus clay: safety report. Demonstration of disposal feasibility (Entsorgungsnachweis) for spent fuel, vitrified high-level waste and long-lived intermediate-level waste. Nagra Technical Report NTB 02-05, Nagra, Wettingen, Switzerland.

OECD/NEA (2008) Radioactive waste management committee: "Collective statement on moving forward to geological disposal of radioactive waste", ISBN 978-92-64-99057-9.

Ondraf (2001) SAFIR 2: safety assessment and feasibility interim report 2. NIROND-2001-06 E. Ondraf, Brussels.

Parkhurst D. L. and Appelo C. A. J. (1999) User's guide to PHREEQC (Version 2) – a computer program for speciation, batch reaction, one-dimensional transport and inverse geochemical calculation. Water-resources Investigation Report 99-4259, USGS, Denver, Colorado, p. 312.

Pearson F. J., Tournassat C. and Gaucher E. C. (2011) Biogeochemical processes in a clay formation in situ experiment: Part E – Equilibrium controls on chemistry of pore water from the Opalinus Clay, Mont Terri Underground Research Laboratory, Switzerland. *Appl. Geochem*. **26**, 990–1008.

Pitzer K. S. (1991). Activity Coefficients in Electrolyte Solutions, CRC Press, Boca Raton.

Ravel B. and Newville M. (2005) ATHENA and ARTEMIS: data analysis for X-ray absorption spectroscopy using IFEFFIT. *J. Synchrotron Radiat.* **12**, 537–541.

Rothe J., Butorin S., Dardenne K., Denecke M. A., Kienzler B., Löble M., Metz V., Seibert A., Steppert M., Vitova T., Walther C. and Geckeis H. (2012) The INE-Beamline for actinide science at ANKA. *Rev. Sci. Instrum.* **83**, 043105.

Rothe J., Denecke M. A., Dardenne K. and Fanghänel T. (2006) The INE-beamline for actinide research at ANKA. *Radiochim. Acta.* **94**, 691–696.

634 Schijf J. and Ebling A. M. (2010) Investigation of the ionic strength dependence of Ulva
635 lactuca acid functional group pK_{as} by manual alkalimetric titrations. *Environ. Sci.*
636 *Technol.* **44**, 1644–1649

637 Schnurr A., Marsac R., Kupcik T., Rabung T., Lützenkirchen J. and Geckeis H. (2015)
638 Sorption of Cm(III) and Eu(III) onto clay minerals under saline conditions: Batch
639 adsorption, Laser-fluorescence spectroscopy and modeling. *Geochim. Cosmochim. Acta*
640 **151**, 192–202.

641 Sjoblom R. and Hindman J.C. (1951) Spectrophotometry of neptunium in perchloric acid
642 solutions. *J. Am. Chem. Soc.* **73**(4), 1744–1751.

643 Vilks P. (2011) Sorption of selected radionuclides on sedimentary rocks in saline conditions –
644 Literature review. NWMO TR-2011-12, Atomic Energy of Canada Limited, Toronto,
645 Ontario, Canada.

646 Zoll A. M. and Schjif J. (2012) A surface complexation model of YREE sorption on *Ulva*
647 *lactuca* in 0.05–5.0 M NaCl solutions. *Geochim. Cosmochim. Acta* **97**, 183–199.

648

Figure caption

Figure 1. Np sorption to illite (log R_d in L kg^{-1}) after 1 week contact time in 1.0 and 3.2 m NaCl versus pH_m for $[Np(V)]_{tot}$ = 10^{-6} M (a) and 5×10^{-8} M (b). The results obtained in 0.1 m NaCl are taken from Marsac et al. (2015a) after 1 week contact time, $[Np(V)]_{tot}$ = 10^{-6} M (a) and 3×10^{-8} M (b).

Figure 2. On the left: experimental log R_d data measured after 1 week versus the pH_m for the various $[Np]_{tot}$ investigated (0.05, 0.09, 0.3, 0.5, 0.9 and 3 µM; shown as different symbols), for m_{NaCl} = 1.0 m (a) and 3.2 m (c). Calculated pH-edges for sorption of Np(V) and Np(IV) (no redox transition considered), respectively, are shown as lines. On the right: corresponding pH_m-pe values measured in m_{NaCl} = 1.0 m (b) and 3.2 m (d) for the different $[Np]_{tot}$ are shown with the same symbols as on the left. The calculated Np(V)/Np(IV) redox borderlines in solution ($\{Np(V)/Np(IV)\}_{aq}$; black line) and at the illite surface ($\{Np(V)/Np(IV)\}_{surf}$; grey line) are also shown. Error bars are not shown for clarity but uncertainties for log R_d (a,c) lie in the range of ± 0.3 and for pe (b,d) in the range of ± 0.8. The pH-pe value for the sample analyzed by XANES (m/V = 20 g L^{-1}; 3.2 m NaCl; $[Np]_{tot}$ = 3×10^{-4} M) is also shown (d).

Figure 3. (a) Np L_3-XANES measured for Np-illite samples ($[Np]_{tot}$ = 3×10^{-4} M, m/V = 20 g L^{-1}) prepared in 0.1 m NaCl (pH_m = 7.4; pe = 6.8; Marsac et al., 2015a) and 3.2 m NaCl (pH_m = 7.9; pe = 7.3; present study). Reference XANES of aqueous Np(IV) and Np(V) in 1 M $HClO_4$ from Gaona et al. (2012) are shown for comparison. Arrows highlight the partial Np(V) reduction to Np(IV) in the present study. The area between 17610 and 17650 eV is enlarged in (b). Results of the linear combination fit are shown in the supporting information (Figure S1).

Figure 4. Np-illite sorption datasets from Marsac et al. (2015a; m_{NaCl} = 0.1 m) and the present study (m_{NaCl} = 1.0 and 3.2 m) are plotted as log R_d versus pe. Lines are calculations made with the 2 SPNE SC/CE model for pH_m = 7 using the surface complexation constants determined by Marsac et al. for Np(IV) (2015a; top dotted line), Banik et al. for Pu(IV) (2016; bold line) or fitting these constants to the 1.0 and 3.2 m NaCl data (bottom dotted curve). The corresponding log R_d(Np(IV)) is given on the y-axis.

Figure 5. Modelled versus experimental log R_d values for Np (data from this study and Marsac et al., 2015a) and Pu in 0.1 < m_{NaCl} < 3.2 m (data from Banik et al., 2016; Marsac et al., 2017). The 1:1 (solid) line is associated with an uncertainty of ± 1.1 log R_d units (dashed lines).

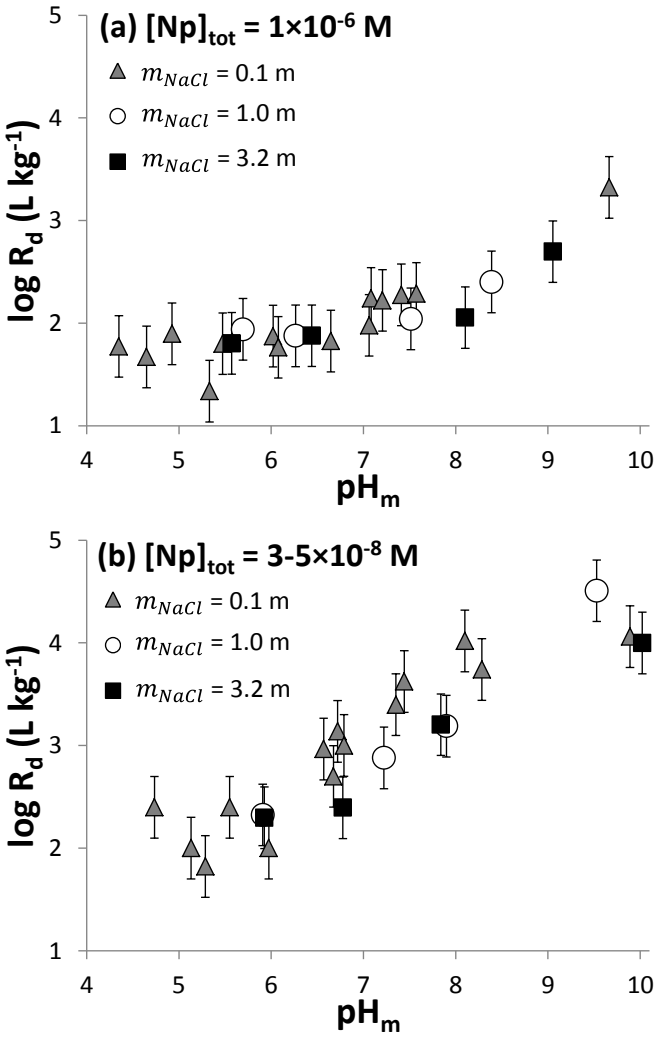

681

682 **Figure 1**

683

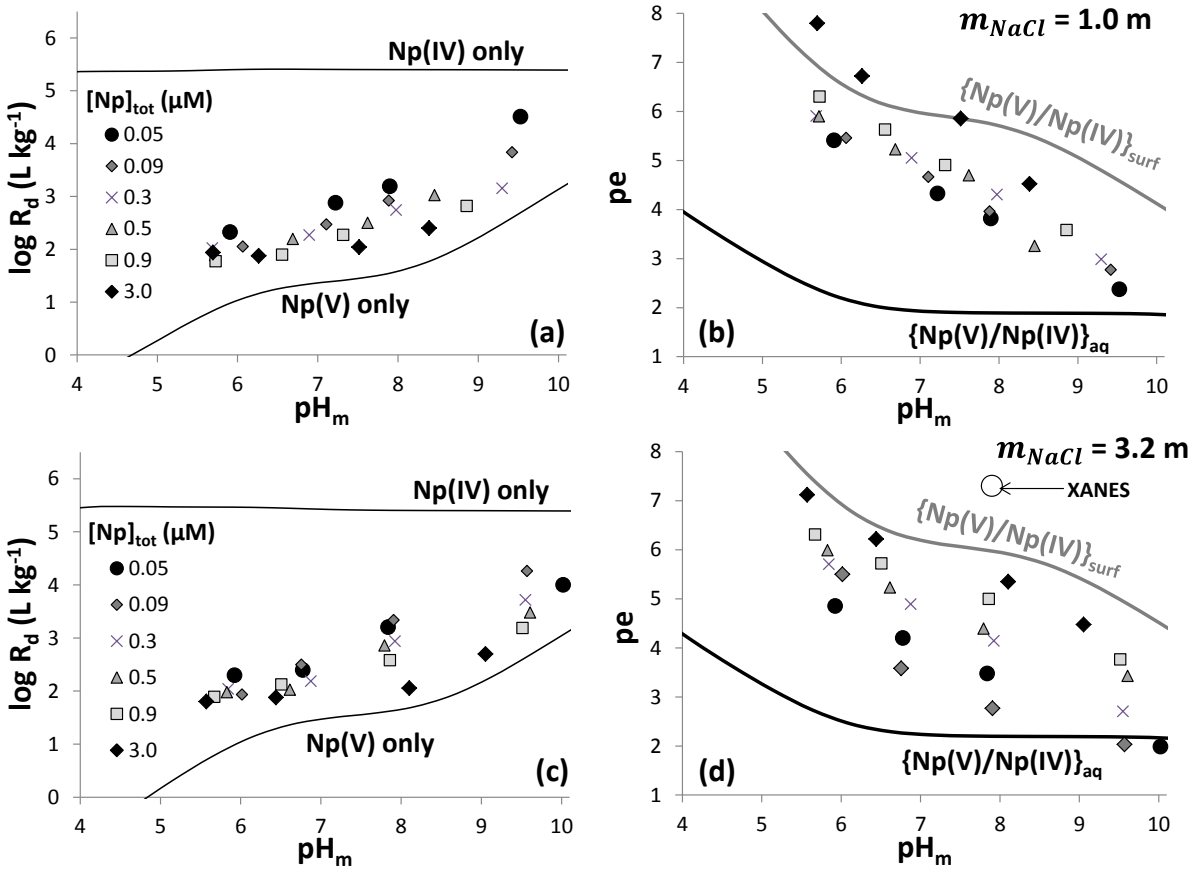

684

685 **Figure 2**

686

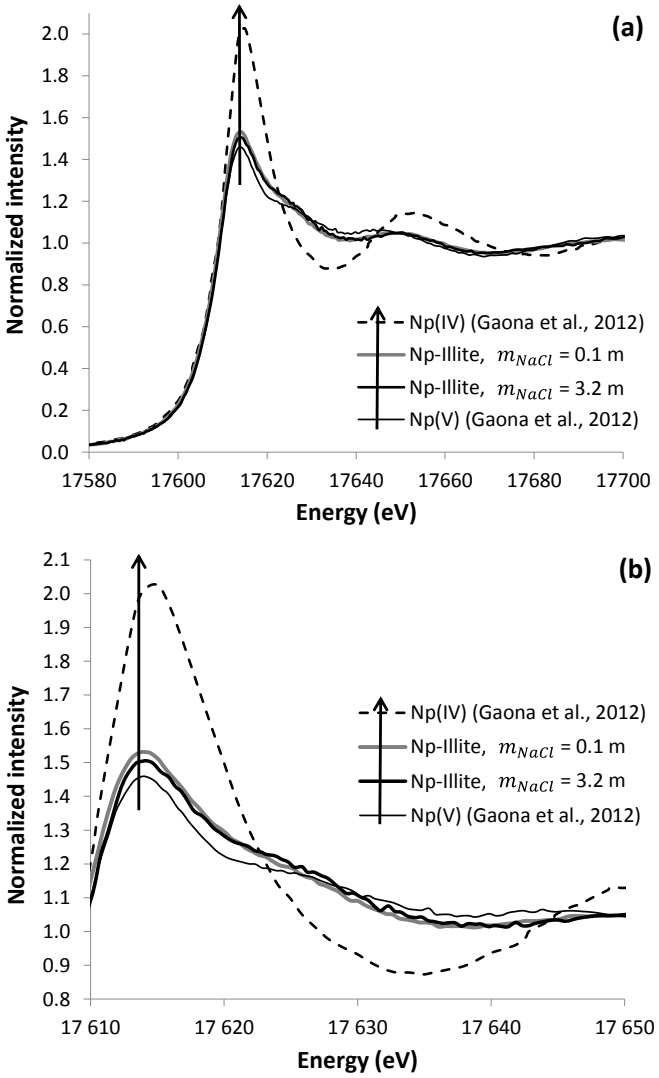

687

688 **Figure 3**

689

690

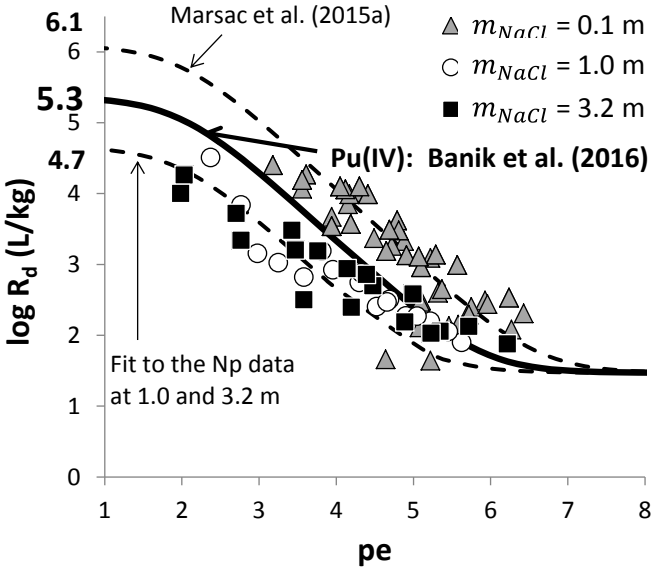

691

692 **Figure 4**

693

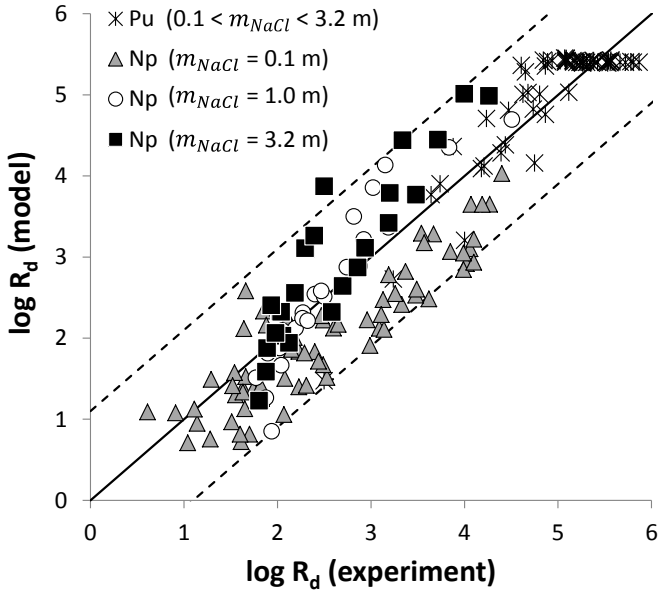

694

695 **Figure 5**